Fault diagnosis in the rotor of squirrel cage induction motor using finite element

M.M.M. Sedky and I.F. ElArabawy
Electrical Engg. Dept., Faculty of Engg., Alexandria University, Alexandria, Egypt
Email: m_mos2004@yahoo.co.uk, Email: Ibr.Arabawy@yahoo.com

Squirrel cage induction motors play an important role in the world's industry. Hence there is a strong demand on their reliable and safe operation. In this paper, the behavior of a three phase induction motors with internal fault condition under sinusoidal supply voltage was examined using Finite Element (FE) model. The concerned fault is rotor broken bars. Different types of broken bars are considered. Two, three, and 4 broken bars cases are studied. Two configurations for each fault are considered; separated and consequtive bars cases are studied. Early detection and diagnosis of these faults are desirable for condition assessment, maintenance, and improved operational efficiency.

يلعب محرك الحث السنجابي ثلاثي الأوجه دورا مهما في الصناعة. ولذلك يوجد تحفظ على مدى فعاليته و تشغيله الأمن. في هذه المقالة يتم اختبار رد الفعل والاستجابة لهذا المحرك تحت حاله من العطل الداخلي مع مصدر جهد متردد. إن أنواع الإعطال الداخلية المختبرة هي وجود كسر في قضبان العضو الدوار بالمحرك. ثلاثة أنواع من الاعطال اختبرت وهى كالتالي: كسر في عدد قضيبين، كسر في عدد ثلاث قضبان، أو كسر في عدد أربع قضبان. و كل عطل تم اختباره على حالتان: الحالة الأولى إن تكون القضبان المكسورة متسلسلة في العدد، والحالة الثانية إن تكون القضبان المكسورة منفصلة عن بعضها البعض. تمت دراسة الاعطاب والحالات المختلفة باستخدام حزمة برمجيات العناصر المحددة. تم دراسة تصرف المحرك تحت الحالات المختلفة من الاعطاب وتم الحصول على نتائج مهمة تساعد في التنبؤ بالاعطاب الحادثة للمحرك في الصناعة.

Keywords: Induction motor, Finite element analysis, Broken rotors, Eddy current

1. Introduction

Nowadays most of the motors used in industry are squirrel-cage induction motors because of their simple design, rugged construction, reliable operation, low initial cost, easy operation and maintenance, and relatively high efficiency. Hence numerous studies were presented in recent years in the field of fault detection of these machines. In general, fault diagnosis of induction motors has focused on sensing failures in one of three major components: stator, rotor, and bearing [1]. In this paper, broken squirrel-cage bars faults are addressed. Well developed fault detection of any electrical machine requires a well-grounded theoretical basis. The use of simulation tools helps the researchers to emphasis the effect caused by faults in an electrical machine, and to develop efficient fault detection methods. Using Finite Element Method (FEM) analysis, the changes in electric, magnetic, and machine behavior due to any fault can be easily observed without the need of dismantling the machine, or testing it in laboratories. Magnetic field distribution within the motor contains full information on the status of stator and rotor of the motor. Evaluation of the magnetic field distribution makes it possible to evaluate the actual performance of the motor [2, 3]. FEM analysis has been coupled to circuit simulation which allows simulating the operating conditions of the induction motor with real power supply connections. Magnetic field distribution within the motor can be evaluated using FEM, based on the dimension and magnetic parameters of the motor. Knowing the magnetic field distribution, other quantities, such as induced voltage waveform, magnetic flux density within the air gap and inductances of different windings of the motor are obtained [4-7].

2. Finite element model of the induction machine

In recent years, the FEM became widely used in the design and analysis of electric machines [8]. Several program packages for magnetic field computation have been

developed: MagNet, Flux2D, Ansys, Femlab, Maxwell.

Based on the well-known Maxwell's equations the FEM based program can compute the magnetic field distribution in any electrical machine, and upon this all the parameters and characteristics of the machine can be easily computed. Maxwell software package was used to perform the required simulation. Table 1 lists the characteristic of the 2 pole, 3 phases, 380 v, Y, 95 hp induction motor.

2.1. Stator slot data

Fig. 1 shows the stator slot shape and its dimensions, table 2.

2.2. Rotor slot data

Fig. 2 shows the rotor slot shape and its dimensions, table 2.

Table 1
Characteristics of the 2 pole, 3 phases, 380 v, Y, 95 hp induction motor.

Number of pole	2
Number of stator slots	36
Number of rotor slots	28
Stator outer diameter (inches)	10.1
	25
Rotor outer diameter (inches)	5.525
Shaft diameter (inches)	1.875
Air gap (inches)	0.046
Stack length (inches)	9.5
Stator and rotor material	Steel type (D23)

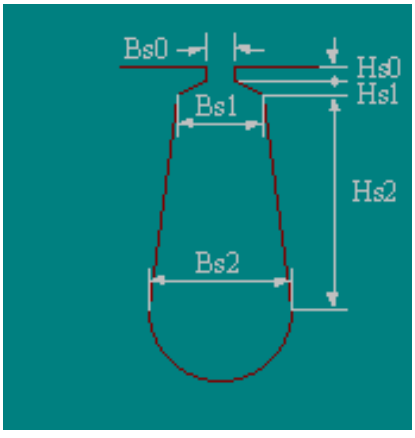

Fig. 1. Stator slot shape.

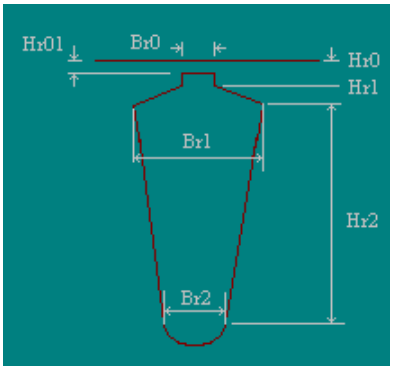

Fig. 2. Rotor slot shape.

Table 2
Stator and rotor slots dimension

Filed stator	Value stator	Filed rotor	Value rotor
Hs0	0.0555	Hr0	0.0215
Hs1	0.065	Hr01	0
Hs2	0.698	Hr1	0.01
Bs0	0.16	Hr2	0.44
Bs1	0.309	Br0	0.01
Bs2	0.432	Br1	0.3
		Br2	0.2

The FEM model of motor geometry is shown in fig. 3. Material properties are assigned to the motor components, where stator windings and rotor bars are considered copper. Stator and rotor body are assigned as steel with the BH curve as shown in fig. 4.

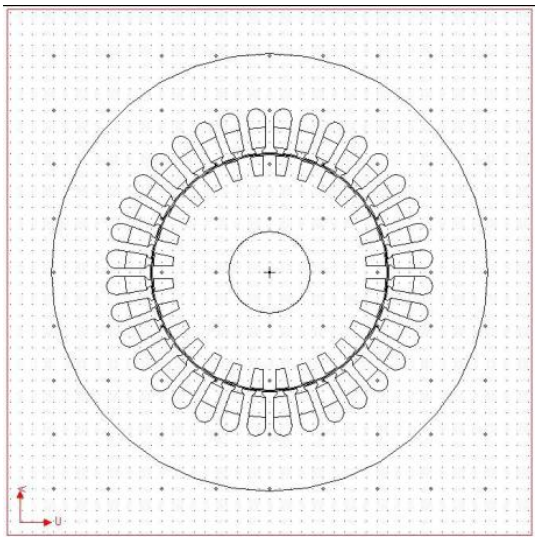

Fig. 3. FEA geometry of induction motor.

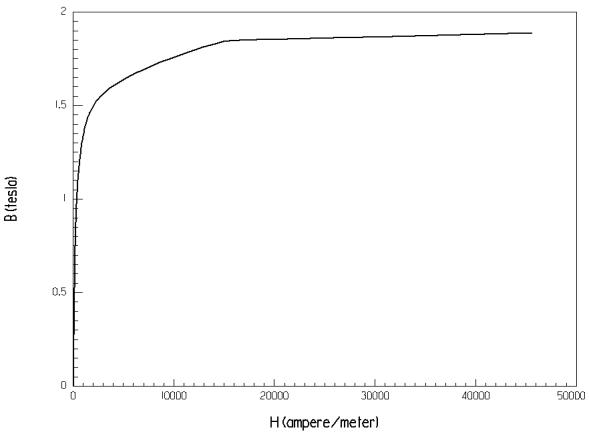

Fig. 4. BH curve of the stator and rotor material.

The Shaft is assigned steel with constant permeability. The air gap between the rotor and stator is assigned air, the region outside the stator is assigned vacuum. In transient solver we need to build a band region to envelop all the rotational parts (rotor, bars, and shaft).

Each phase of the stator three phase sources is divided into two groups, for go and return current. Phase A has PHAgo and PHAret, phase B has PHBgo, and PHBret, phase C has PHCgo and PHCret. Rotor bars are connected all as one group. The whole model is discredited into small elements, where the more elements used, the more accurate solution is obtained. Fig. 5 shows the mesh model of the induction motor.

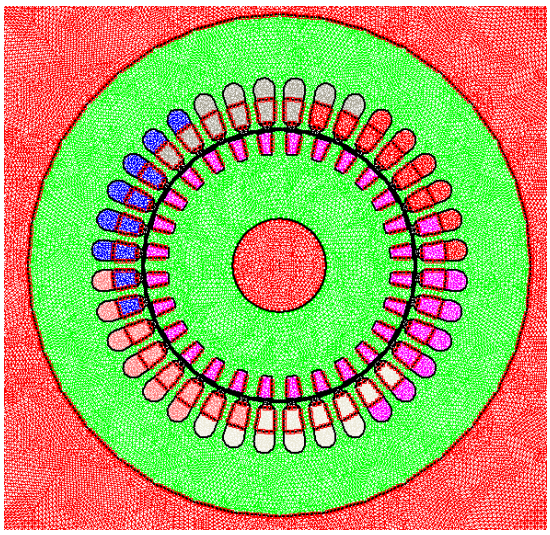

Fig. 5. Mesh distribution of the FEA model.

2.3. Circuit modeling

All stator and rotor conductor areas are represented in the circuit domain of FEM analysis. Stator windings are assigned as stranded conductors, with relevant resistances and inductances assigned to each phase. In the circuit schematic diagram stator windings are assigned in star connection with three phase supply applied to them. Fig. 6. shows the three phase winding of the stator winding. Rotors bars are considered as parallel winding, (for the squirrel cage case). Broken bars are assigned as a solid current source with total current equals zero, which is to represent the breaking effect of the bar.

3. Maxwell's equations

The transient solver of the FEM analysis allows solving and analyzing the magnetic fields, energy, force, power, power loss, speed, and flux of the model at various time steps of the solution over a specified period of time. It allows a non sinusoidal current or voltage excitation as well as rotational or translational motion. The transient solver of the FEM analysis assumes the following conditions about the problem:

1. If motion occurs in the model, no motion occurs outside the band object.
2. Only one type of motion (translational or rotational) occurs in the model.
3. More than one object can be assigned identical motion within the band object.

The time-dependent magnetic filed eq. [9] is expressed in eq. (1)

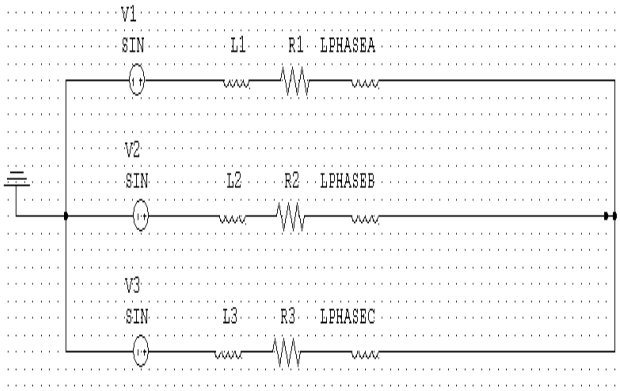

Fig. 6. The external electric circuit of the stator circuit.

$$\nabla \times \upsilon \nabla \times A = J_s - \sigma \frac{\partial A}{\partial t} - \sigma \nabla v + \nabla \times H_c + \sigma v \times \nabla \times A, \quad (1)$$

Where,
H_C is the coercivity of the permanent magnet,
v is the velocity of the moving parts,
A is the magnetic vector potential, and
J_s is the source current density.

The transient solver applies a reference frame that is fixed with respect to the components in the model by setting the velocity, υ, equal to zero. Because the moving components have now been fixed to their own coordinate system, the partial time derivative becomes in the total time derivative of A. Thus, the motion equation becomes:

$$\nabla \times \upsilon \nabla \times A = J_s - \sigma \frac{dA}{dt} - \sigma \nabla v + \nabla \times H_c . \quad (2)$$

The induction motor has two types of current source; stranded and solid. Stator winding are assigned as a stranded current source, where stranded conductors lack eddy current behavior and are considered to be filaments too thin to model in a practical finite element grid. Because of this, the transient solver assumes that their contribution to the current density is averaged over the area of problem region. The current density is based on eq (3).

$$\nabla \times \upsilon \nabla \times A = J_s . \quad (3)$$

Rotor bars are assigned parallel solid conductor, where solid conductor is large enough to model with finite element. The skin effect depends not only on the frequency of the systems, but also on the location of nearby conductors. Based on Ampere's law, the total current density, J_t, in the system is given by eqs. (4, 5 and 6). For the broken bars the total current density is equal zero.

$$J_t = J_e + J_s . \quad (4)$$

Where,

$$J_t = -\sigma \frac{\partial A}{\partial t} - \sigma \nabla v . \quad (5)$$

Which it reduces to

$$J_t = -\sigma \frac{\partial A}{\partial t} + \frac{\sigma}{l} V_b , \quad (6)$$

Where,
V_b is the voltage difference across the conductors end points,
J_e is the eddy current density, and
Js is the source current density.

3.1. Rotational motion

The transient motion simulator generates rotational motion based on the following motion equation, eq (7).

$$J\beta + D\omega = T_{comp} + T_{load} . \quad (7)$$

Where,
J is the inertial force, in kg.m^2,
T is the torque, in N.m,
ω is the angular speed, in rad/sec,
β is the angular acceleration, in rad/sec^2, and
D is the damping factor, in N.m.s.

4. Simulation results

In order to simulate the internal faults, geometry modification as well as circuit modification is necessary. The broken bars are realized by assigning the broken rotor bars as a solid current source with zero current, where there is no source current passing on it. But, there will be surface induced eddy current in it. The transient solver helps us to investigate the magnetic flux distribution in the air gap during transient as well as steady state conditions. The machine behavior under broken bars faults was investigated under sinusoidal voltage source. Different types of broken bars faults are investigated. Two broken bars and four broken bars were investigated, in two distribution manner, separate broken bars and sequential broken bars.

4.1. Starting simulation

Simulation results are investigated at starting and steady state conditions, where it is expected that the big effect will be at starting.

Fig. 7 shows the flux distribution for healthy motor at transient, at t = 0.051 sec. Healthy case will be the reference for all other cases.

Figs. (8-a, b, c, d) show the flux distribution under different number of broken bars and different locations, at the same time of the investigated healthy motor. In the case of broken bars, the magnetic field is no longer sinusoidal around the circumference of the air-gap due to lack of the induced currents in the broken bars. Also the broken bars are considered as a flux barrier now due to the surface induced currents in them. Also for sequential broken bars, they have great effect in distorting the air gap flux more than if the broken bars are separate from each others.

The magnetic flux distribution is fundamentally altered during broken rotor bars fault. Fig. 9-a - d show the magnetic vector potential distribution around the contour located at the bottom of the rotor bars. And fig. 10-a - d shows the magnetic vector potential distribution around the contour located at the top of the rotor bars.

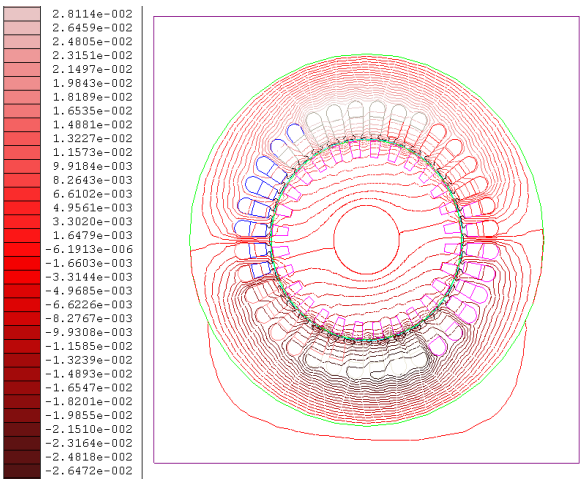

Fig. 7. Magnetic flux distribution for healthy motor.

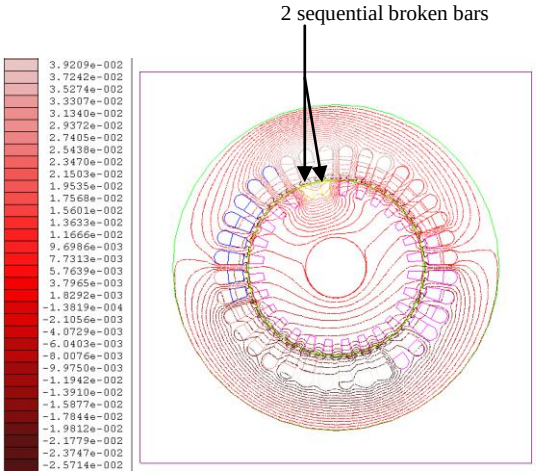

Fig. 8-a. Magnetic flux distribution for two sequential broken bars.

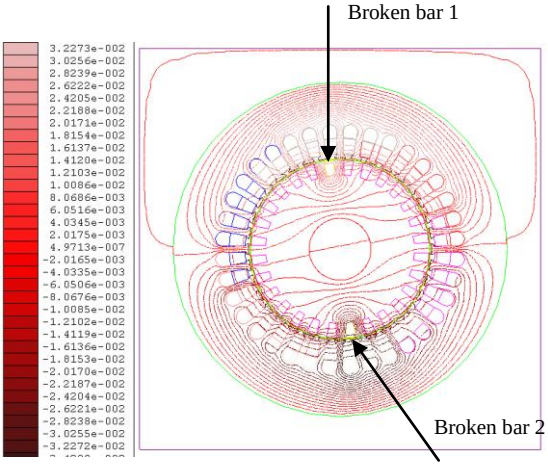

Fig. 8-b. Magnetic flux distribution for two separate broken bars.

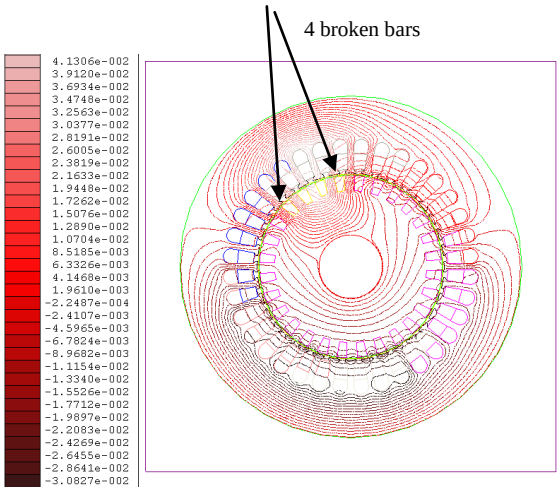

Fig. 8-c. Magnetic flux distribution for four sequential broken bars.

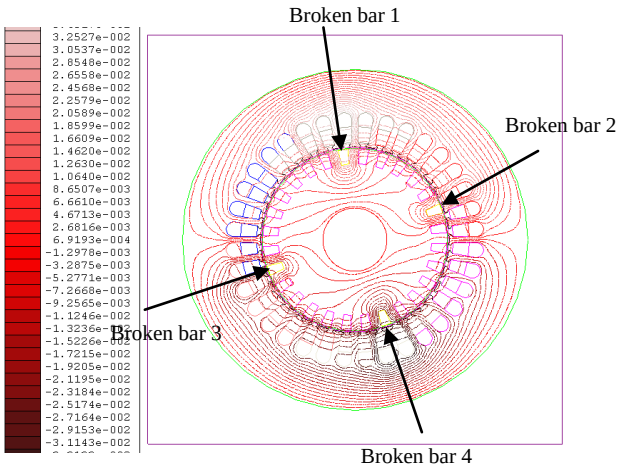

Fig. 8-d. Magnetic flux distribution for four separate broken bars

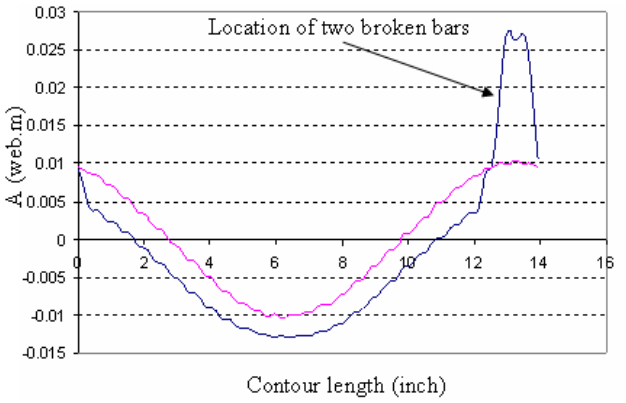

Fig. 9-a. Magnetic vector potential for 2 sequential broken bars.

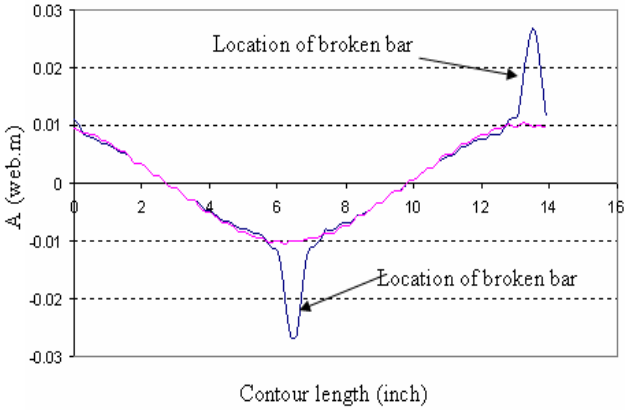

Fig. 9-b. Magnetic vector potential for 2 separate broken bars.

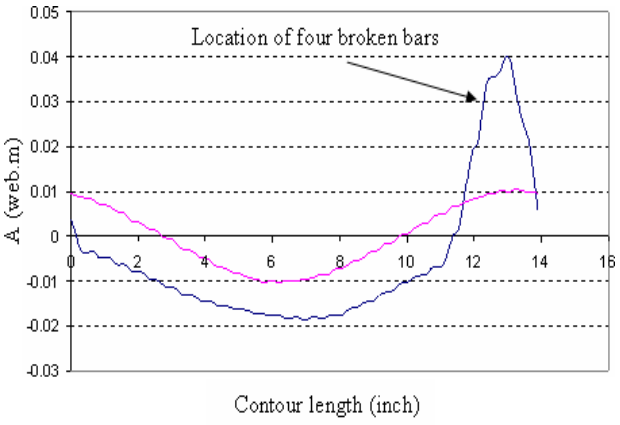

Fig. 9-c. Magnetic vector potential for 4 sequential broken bars.

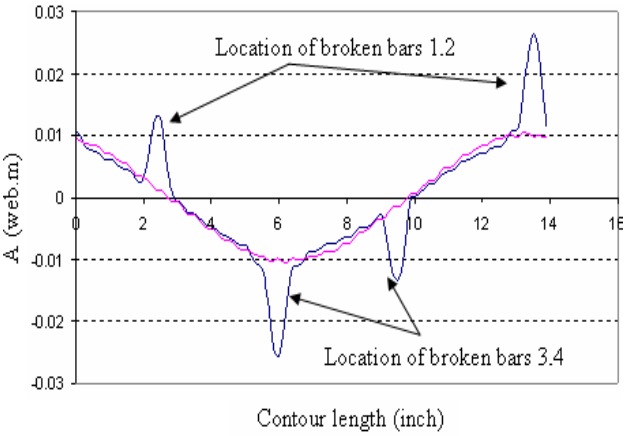

Fig. 9-d. Magnetic vector potential for 4 separate broken bars.

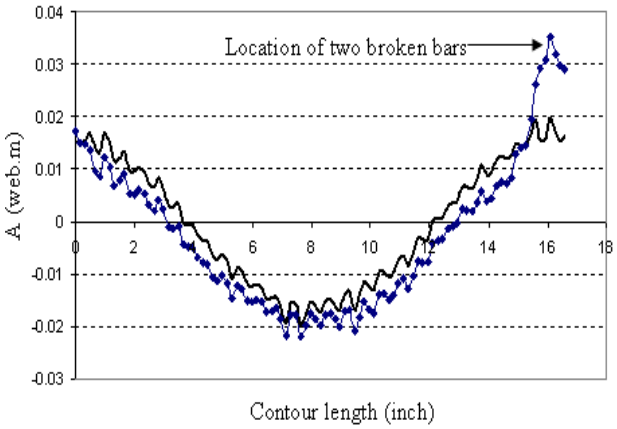

Fig. 10-a. Magnetic vector potential for 2 sequential broken bars.

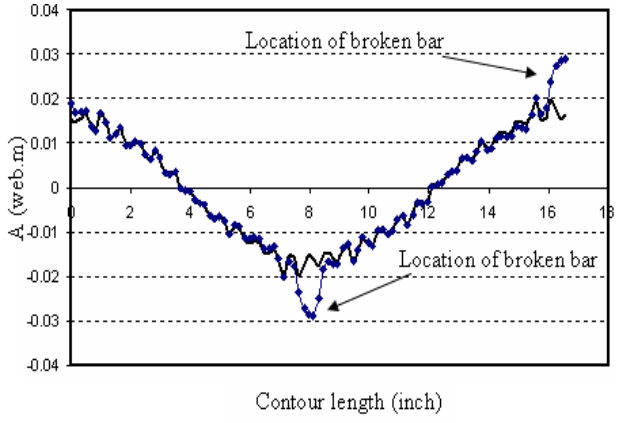

Fig. 10-b. Magnetic vector potential for 2 separate broken bars.

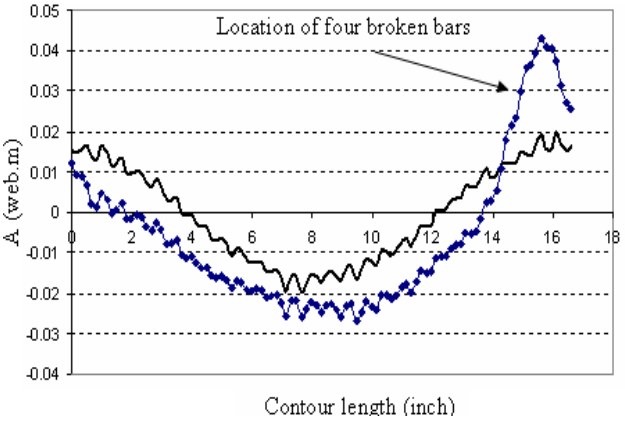

Fig. 10-c. Magnetic vector potential for 4 separate broken bars.

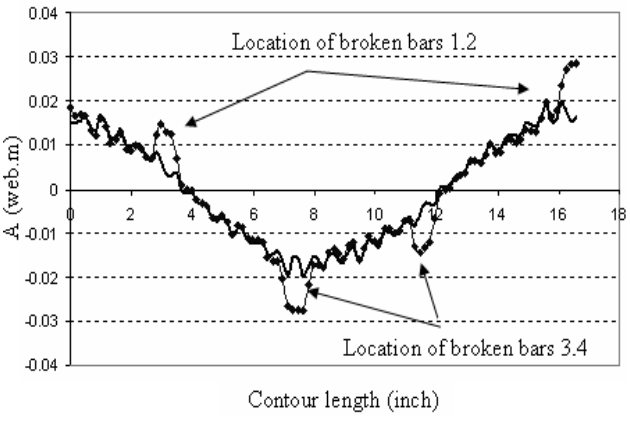

Fig. 10-d. Magnetic vector potential for 4 separate broken bars.

4.2. Steady state simulation

Simulation results for the magnetic distribution at steady state are investigated at t = 0.1 sec. Fig. 11 show the magnetic flux distribution at t = 0.1 sec. The magnetic flux distribution is not distorted due to the broken bars. This means that the broken bars have no effect after transient period, where the current is in the steady state. Broken bars are working as a flux barrier in the transient period only.

Transient simulation for the developed torque and stator current give clear investigation about the effect of the broken bars in the starting period and steady state period. Fig. 12-a-d shows the developed torque generated at different cases for broken bars, comparing with developed torque at healthy case which are investigated in related to the magnetic flux distribution. Fig. 12-a shows that at starting there is difference between the healthy case and the one with two sequential broken bars. An extra torque is observed due to the reluctance torque which is developed due to the 2 broken bars, (this is due to the non-homogenous of the air gap now). The two broken bars are working as a flux barrier now, which cause reluctance torque due to the no-uniform air gap now. At steady state there is no effect of the broken bars on the developed torque that is what is shown in the flux distribution. Comparing between 2 sequential broken bars and 2 separate broken bars, 2 sequential broken bars have effect more than the two separate broken bars. Fig.12-c, d show the developed torque for 4 broken bars compared with the healthy case.

As approved for 2 broken bars, four sequential broken bars have more effect that the two broken bars. There is a pulsating torque appearing in the case of 4 broken bars, in the steady state period, while there is drift in the transient torque compared by the healthy case. In this case we find that the sequential broken bars have big effect that the separate bars.

Transient currents for the stator are investigated and analyzed by FEM. Fig.13-a-d, show the transient current for phase A for healthy motor and defected motor with the broken bars.

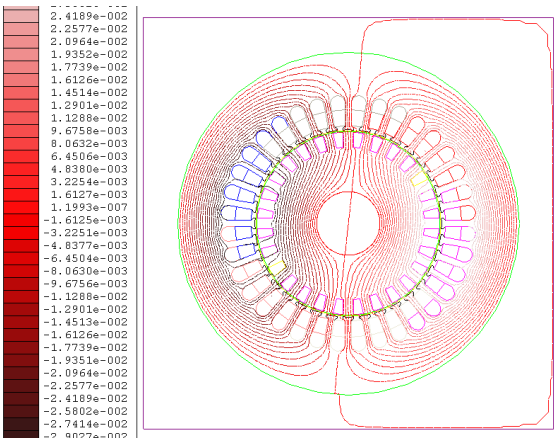

Fig. 11-a. Magnetic flux distribution at steady state t=0.1 sec for 2 separate broken bars.

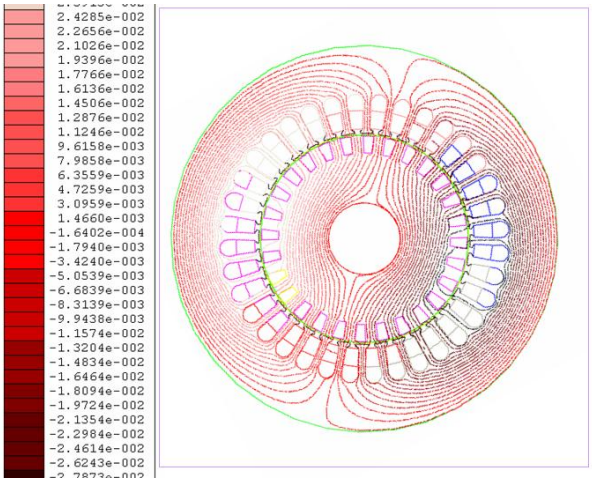

Fig. 11-b. Magnetic flux distribution at steady state t=0.1 sec for 2 sequential broken bars.

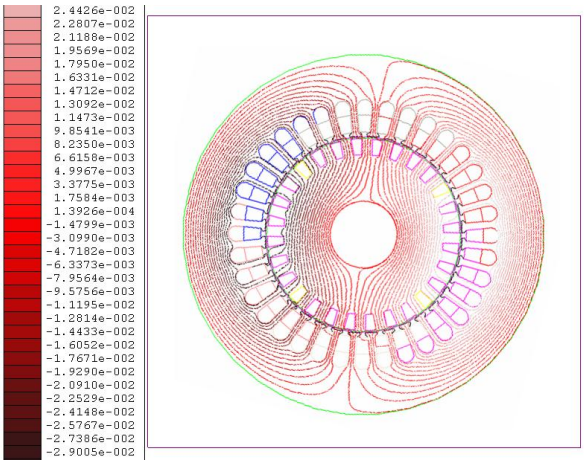

Fig. 11-c. Magnetic flux distribution at steady state t=0.1 sec for 4 separate broken bars.

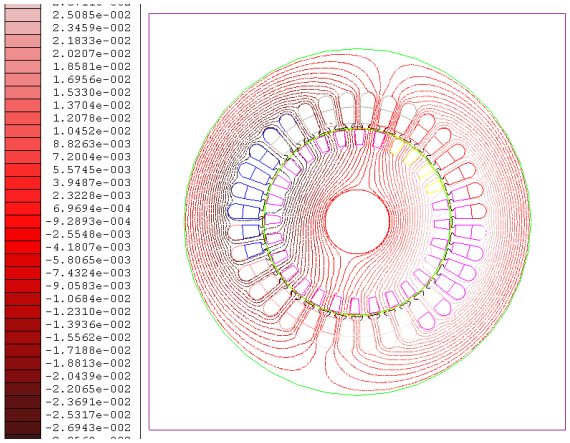

Fig. 11-d. Magnetic flux distribution at steady state t=0.1 sec for 4 sequential broken bars.

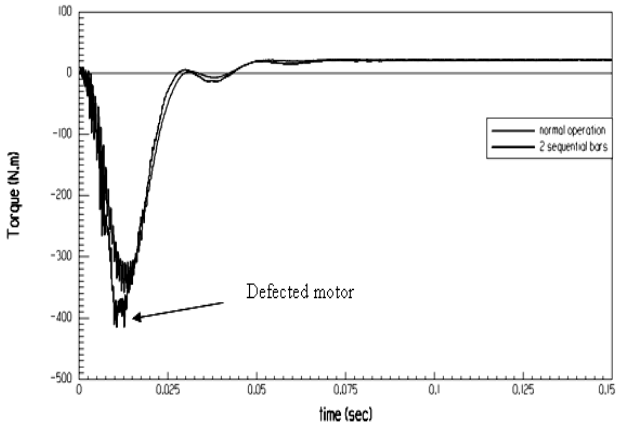

Fig. 12-a. Developed torque for 2 sequential broken bars.

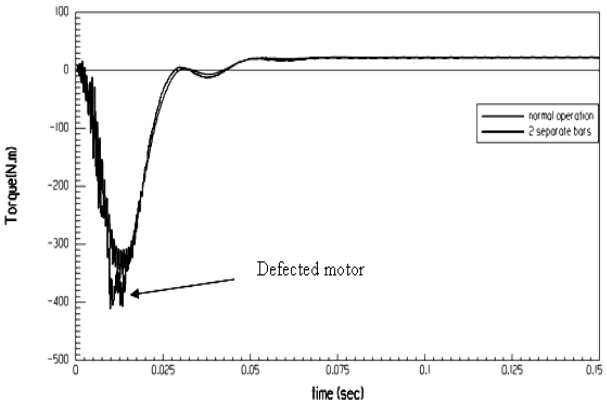

Fig. 12-b. Developed torque for 2 separate broken bars.

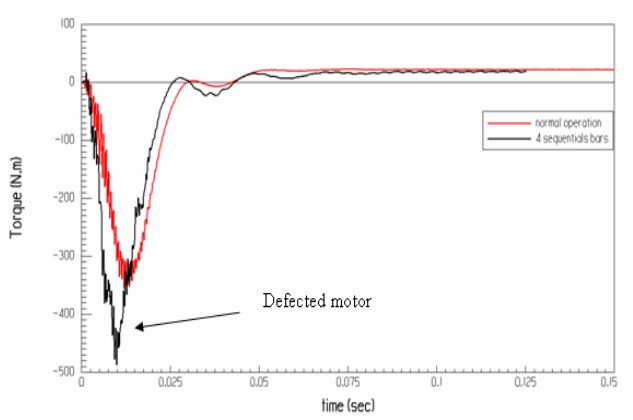

Fig. 12-c. Developed torque for 4 sequential broken bars.

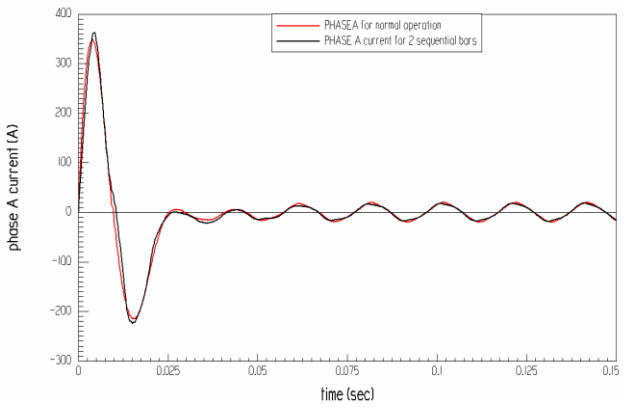

Fig. 13-b. Transient phase current for healthy and 2 sequential broken bars.

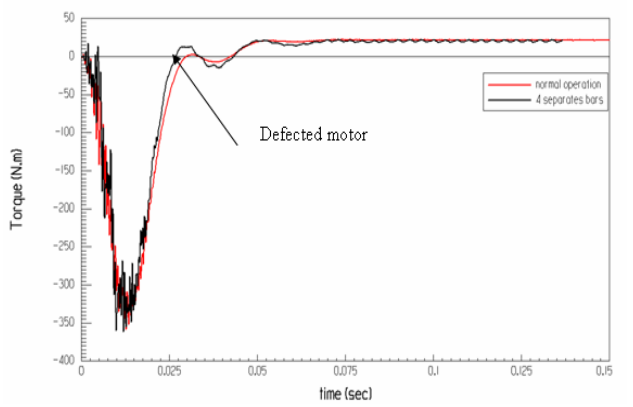

Fig. 12-d. Developed torque for 4 separate broken bars.

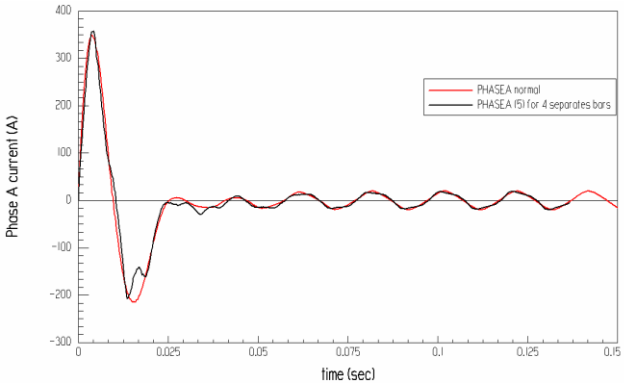

Fig. 13-c. Transient phase current for healthy and 4 separate broken bars.

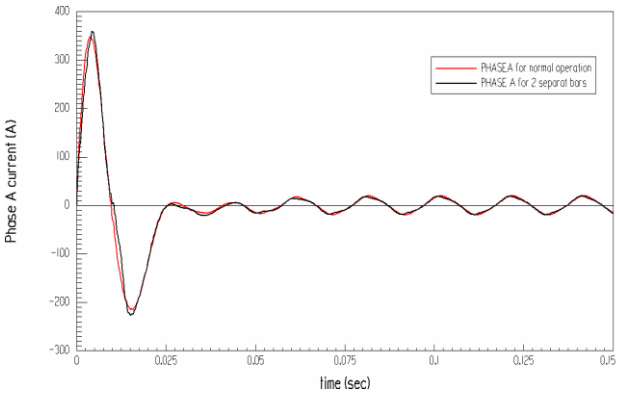

Fig. 13-a. Transient phase current for healthy and 2 separate broken bars.

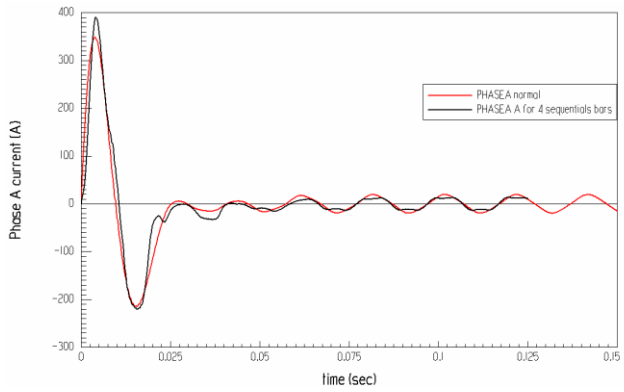

Fig. 13-d. Transient phase current for healthy and 4 sequential broken bars.

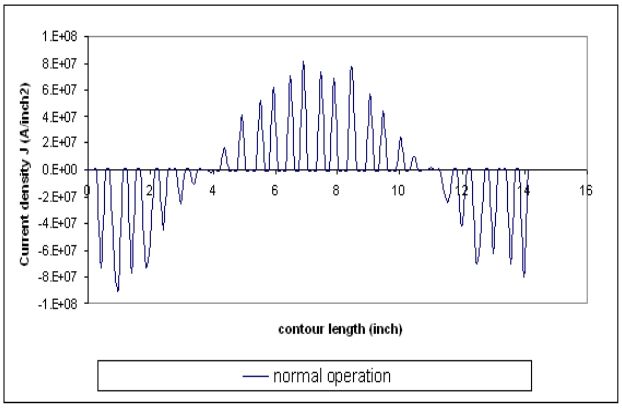

Fig. 14-a. Current density in the rotor bars for healthy.

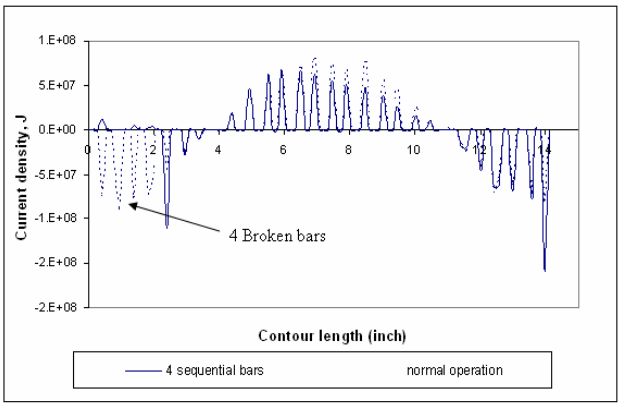

Fig. 14-d. Current density in the rotor bars for 4 sequential broken bars.

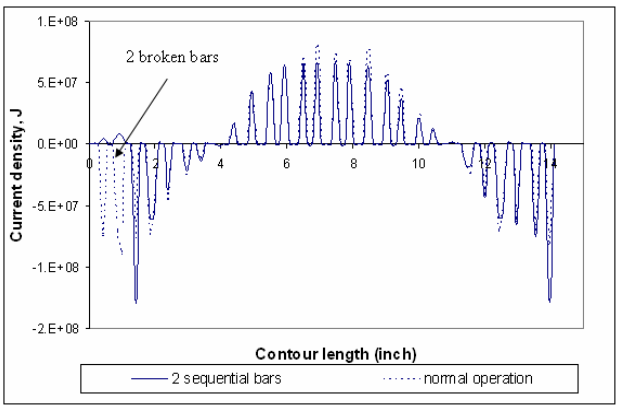

Fig.14. b. Current density in the rotor bars for 2 sequential broken bars.

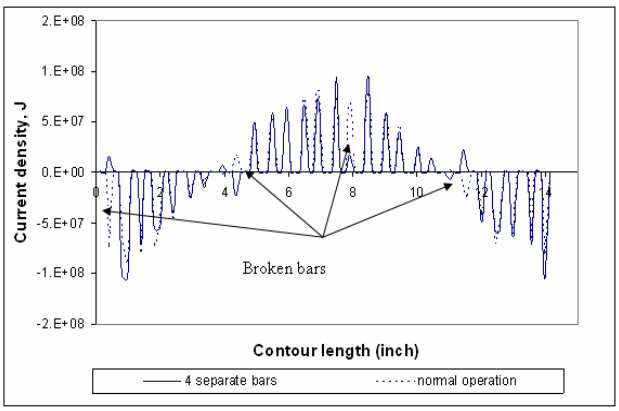

Fig. 14-e. Current density in the rotor bars for 4 separate broken bars.

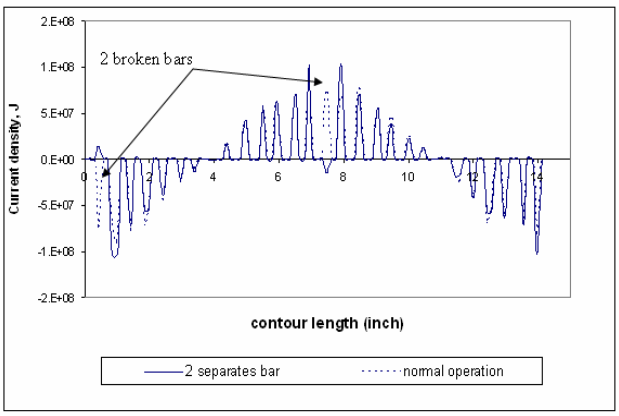

Fig. 14-c. Current density in the rotor bars for 2 separate.

In the case of sequential bars, the current is higher than the current of healthy motor. And at steady state there is little distortion of the phase current, where it is not pure sinusoidal in this case. Broken bars cause the flux to be diverted around those bars, causing the current to increase in the neighbors bars. These increasing current causes thermal effect in the adjacent bars and may cause another failure of them if the problem is not solved. Fig. 14 a-d show the current density in the rotors bars compared with the healthy machine. This current density is investigated around a contour passing in the middle of the rotor bars. The increase of the current density in the neighboring bars is well shown in the figures for all the cases. Sequential broken bars case still has the dominate effect than the separate broken bars.

In the study of induced eddy current in the neighbors' bars of the broken bars, current density is investigated at transient period at t= 0.005 sec.

Using FEM proves that the rotors bars next to the broken ones are the most exposed to future damage, due to their very high current density, and it can be expected that the fault will soon propagate to these overloaded bars.

5. Conclusions

This paper has presented the utilization of FEM in diagnosis of the flux distribution in the three phase squirrel cage induction motor, under internal fault of broken bars. Using FEM, most of the typical fault of the machine can be studied. Using FEM proves that the rotor bars next to the broken ones are the most exposed to future damage, due to their very high current, and it can be expected that the fault will soon propagate to these overloaded bars.

It is proved also that steady state analysis of the induction motor doesn't change that much in the fault case. The faults can be detected from the transient simulation, which can not be simulated using convention model. FEM is a powerful tool to simulate the transient condition of any machine and different faults can be detected.

References

[1] A.H. Bonnet and G.C. Soukup, "Cause and Analysis of Stator and Rotor Failures in Three-Phase Squirrel-Cage Induction Motors", IEEE Trans. Ind. Application., Vol. 28 (4), pp. 921-037 (1992).

[2] A.M. Trzynadoosky, "Diagnostic of Mechanical Abnormalities in Induction Motor Using Instantaneous Electrical Power", Proceeding of the 1997 International Electric Machines and Drives Conference, Milwaukee, pp. 91-93 (1997).

[3] J. Faiz and B.M. Ebrahimi, "Mixed Fault Diagnosis in Three-Phase Squirrel-Cage Induction Motor Using Analysis of Air-Gap Magnetic Field", Process in Electromagnetic Research, PIER 64, pp. 239-255 (2006).

[4] M.P. Krefta and O. Wasynczuk, "A Finite Element Based State Model of Solid Rotor Synchronous Machines", IEEE Transactions Energy Conversion, Vol. EC-2 (1), pp. 21-30 (1987).

[5] S.C. Ho, C.G. Hong and G.J. Hwang, "Transient and Steady State Performance of a Squirrel-Cage Induction Motor", IEE Proceedings, Vol. 136 (3), pp. 136-142 (1989).

[6] S. Williamson, L.H. Lim and A.C. Smith, "Transient Analysis of Cage Induction Motor Using Finite Elements", IEEE Trans. Magnetic, Vol. 26 (2), pp. 941-944 (1990).

[7] O.V. Thorsen and M. Dalva, "Failure Identification and Analysis for High Voltage Induction Motors in Petrochemical Industry", IEEE Trans. Ind. A, Vol. 12 (2) (1998).

[8] K. Hameyer and R. Belmans, "Numerical Modeling and Design of Electrical Machines and Devices", WIT Press, Southampton (1999).

[9] Li Weili, Xie Ying, Shen Jiafeng and Luo Yingli, "Finite Element Analysis of Field Distribution and Characteristic Performance of Squirrel Cage Induction Motor with Broken Bars", IEEE Transactions on Magnetic, Vol. 43 (4), pp. 1537-1540 (2007).

Received July 26, 2008
Accepted March 30, 2009